High Altitude Turbine Survey: lessons learned from initial design through first flight

P.McGarey, A.Kaczamarowski, S.Saripalli

Arizona State University, School of Earth & Space Exploration (SESE) PO Box 871404 Tempe, Arizona 85287-1404, USA

ABSTRACT

The High Altitude Turbine Survey (HATS) analyzes the relationship between performance characteristics and altitude for micro-propellers. The survey collects thrust and efficiency data as well as environmental information along a vertical profile up to 38 km in altitude. Senors include strain and pressure gauges, thermocouples, and an ultrasonic mutli-axis anemometer. HATS interfaces with the High Altitude Student Platform (HASP), a program funded by the National Aeronautics and Space Administration Balloon Program Office (NASA BPO) and the Louisiana Space Consortium (LaSpace). HATS provides a test-bed for various types of propellers in order to aid in the optimization of airfoil design research for high altitudes. The development of high altitude turbine test platforms and airfoil optimization studies have a wide range of application towards airborne wind energy generation and propeller-driven airships operating at extended altitudes. Data collected during the September 2012 initial flight is correlated to theoretical efficiency models used to determine propeller performance at altitude. The payload concept, design, and engineering outcomes are also discussed.

CONTENTS

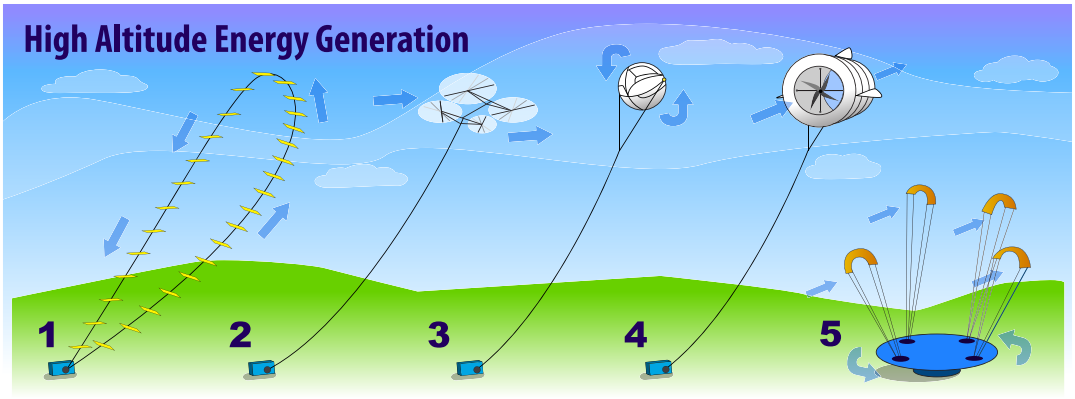

Figure 1. Alternatives for Airborne Wind Energy (1-Ladder Mill 2-Rotorcraft 3 Dirigible 4-Inflatable Propeller 5-Kite Power) rep.[3]

1. SCIENTIFIC BACKGROUND

Wind energy has been used for many years to help offset energy demands and provide access to power generation in remote areas. Unfortunately, traditional wind energy is often geographically limited, and suffers from highly variable wind speeds. As a result, seasonal changes in wind and weather conditions drastically reduce the performance and reliability of wind energy [1]. Studies by the National Centers for Environmental Prediction and the Department of Energy have been conducted to analyze high altitude wind speeds. Figure 2 illustrates the results of one such study [9]. In general, it can be seen that high altitude winds, which include winds at altitudes higher than 500m, have greatly reduced variability, speeds an order of magnitude higher than surface winds, and widespread geographic invariability allowing for end user proximity [9]. The available power density for high altitude winds exceeds 10 kW/m^2, which is larger than many other renewable energy sources such as solar power, ocean currents, or geothermal [9].

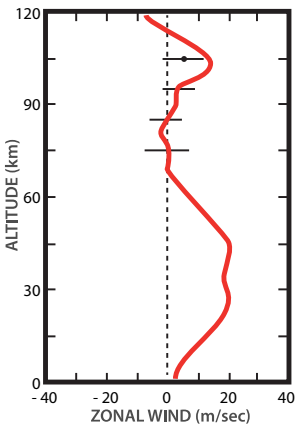

Figure 2. Wind Speeds at Altitude, rep.[5]

Although the potential benefit is great, the technology necessary to capture this energy is still in the early developmental stages. There are five primary methods proposed for the conversion of wind energy, shown in Figure 1. Each method involves the use of a moored aerodynamic surface, be it rotorcraft, kite, or dirigible, to produce a rotational moment that can be converted into energy. Numerical models and conceptual studies have been performed in order to identify possible benefits or issues with each design [2]. Various technology limitations have been identified including energy transmission, power generation efficiency, and longevity of the aircraft at altitude [2]. Researchers are beginning to conduct full-scale system tests for many of the various design schemes. In July 2010 and December 2011, Sky WindPower demonstrated a full-scale rotorcraft capable of lifting off the ground, hovering, and generating transmissible power from a height of 10 meters [17]. Similarly, as recently as March 2012, Altaeros Energies launched a full-scale high altitude aerostat turbine design to approximately 100 meters [12]. These technology demonstrations indicate that the industry for airborne wind energy is growing rapidly and the need for more optimized designs is apparent. Altaeros Energy, for example, currently uses an off-the-shelf Southwest Wind Power SkyStream Turbine airfoil [12], which is optimized for ground level installations no higher than 16 meters [18]. New companies will spend more time and energy addressing engineering challenges related to aerostat, transmission tether, and grid integration technology. The overarching aim of this turbine study is provide companies, like Altaeros, with a high altitude airfoil performance database, which with time and continued analysis, could be used to maximize energy capture at extended altitudes. Whether flexible or rigid, inflatable or kite based, any aerodynamic surface needs to be designed with respect to its operation environment. High altitude wind energy generation research is in its earliest development phase, and accordingly, will require a concerted effort towards optimization and design efficiency.

2. RESEARCH OBJECTIVES

The greatest potential for airborne wind energy generation is associated with tethered rotorcraft [9]. This project addresses the primary engineering concern in developing these wind turbines; the ability to efficiently collect wind power at the lower atmospheric densities. The aerodynamic efficiency of common turbine airfoils is not applicable to jet stream uses. Airfoil optimization is therefore necessary for energy capture at extended altitudes where increased wind speeds with reduced variability exist.

The development of a platform that can assess turbine airfoil thrust efficiency with respect to height is an essential first step. Initially this platform can be used to verify the performances of miniaturized airfoil types optimized for different altitude regimes. Being that propellers are generally not scalable, such tests will serve only to verify thrust data collection methodologies. However, with a larger platform and full scale turbines, the sensory package can be refined to accurately test conceptual high altitude turbine airfoil prototypes. This process would begin with computational fluid dynamic (CFD) modeling of airfoil performance in varying altitudinal regimes, continue with the verification of those models in wind tunnel tests, and conclude with identification of ambient condition effects on turbines in actual flight conditions. The data produced in this type of research, along with any tools built to utilize or extrapolate it, providing information on additional or new airfoil characteristics desired for high altitude environments, will facilitate the development of high altitude wind turbines. Airfoil performance data will also be available for a variety of military and commercial applications including micro-aerial vehicles (MAVs), airship-to-orbit concepts such as those being pursued by JP Aerospace [13], and long duration vehicles for surveillance purposes. Research surrounding the use of propeller-driven high altitude airships for surveillance, communication, and atmospheric research could greatly benefit from a systematic analysis of propeller response to altitudinal atmospheric conditions.

3. THEORY OF PROPELLER EFFICIENCY

According to Froude's momentum theory of propulsion, the change in energy across a propeller or wind turbine is the result of a change in the momentum of air across the propeller. In this sense, the difference between a propeller and a turbine is simply that one imparts energy to the air and the other extracts that energy. Figure 3 demonstrates a basic propeller system, where the propeller is assumed to be a thin disc that imparts an increase in pressure to the air.

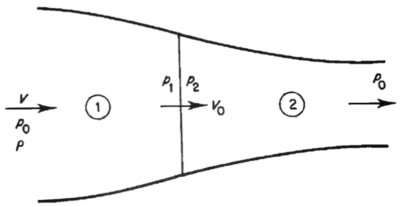

Figure 3. propeller as thin disk [7]

In this system, the thrust on the propeller is the increase in reward momentum of the mass of air accelerated through the propeller and is defined in Equation 1.

$$T = \rho S V_0 (V_s - V) \tag{1}$$

Where S is the area covered by the propeller and ρ is the density of the air. Thrust can also be expressed in terms of the pressures on either side of the propeller as shown in Equation 2.

$$T = S(p_2 - p_1) \tag{2}$$

The efficiency of a propeller in this system is defined as the rate at which the propeller does work on the air divided by the rate of increase of energy of the air. The propeller work rate is a function of its thrust and axial velocity. The rate of energy change in the air is its change in kinetic and pressure energy. Therefore, the efficiency of a propeller is given by Equation 3.

$$\eta = \frac{TV}{\frac{1}{2}\rho S V_0 (V_s^2 - V^2}) \tag{3}$$

The efficiency of a propeller can also be defined as a function of the inflow factor a as shown in Equation 4.

$$\eta = \frac{1}{1+a} \tag{4}$$

Where a is defined by Equation 5 and 6.

$$V_0 = V(1+a) \tag{5}$$

$$V_s = V(1+2a) \tag{6}$$

Using Bernoullis equation for incompressible fluid flow, the inflow factor can be defined in terms of the pressure difference across the propeller as shown in Equation 7.

$$a = -1 + \frac{1}{2}\left(4 + \frac{2(p_2 - p_1)}{\rho V}\right)^{\frac{1}{2}} \tag{7}$$

From Equation 7, an equation of propeller efficiency as a function of the change in pressure due to the propeller is given in Equation 8.

$$\eta = \frac{2}{\left(4 + \frac{2(p_2 - p_1)}{\rho V}\right)^{\frac{1}{2}}} \tag{8}$$

While the momentum theory of propellers is a very simple model for propeller efficiency, it can be seen that there will be an inherent relationship between altitude and propeller efficiency as shown by the density term in Equation 8. In order to understand how propeller efficiency will change as a function of altitude, one needs to understand how density changes as a function of altitude. From the ideal gas law and a lapse rate relationship between temperature and height, the relationship between pressure and altitude can be found as given in Equation 9.

$$\rho = p_0 \left(1 - \frac{L \cdot h}{T_0}\right)^{\frac{gM}{RL}} \tag{9}$$

Where h is the altitude above sea level in meters, L is the lapse rate (approximately 0.0065 K/m), p_0 (101.325 kPa) and T_0 (288.15 K) are the pressure and temperature under standard atmospheric conditions respectively, M is the molar mass of dry air (approximately 0.0289644 kg/mol), g is the acceleration due to gravity (approximately 9.80665 m/s^2), and R is the universal gas constant (approximately 8.31447 J/(mol*K)). Density as a function of altitude can then be calculated from Equation 10.

$$\rho = \frac{M p_0}{RT}\left(1 - \frac{L \cdot h}{T_0}\right)^{\frac{gM}{RL}} \tag{10}$$

Therefore, a general relationship for propeller efficiency as a function of altitude can be described as in Equation 11.

$$\eta = \frac{2}{\left(4 + \frac{2(p_2 - p_1)}{\frac{VMp_0}{RT}\left(1 - \frac{L \cdot h}{T_0}\right)^{\frac{gM}{RL}}}\right)^{\frac{1}{2}}} \tag{11}$$

While there were several assumptions made in order to identify the relationship between propeller efficiency and altitude as given in Equation 11, it can be seen that, even for this simple model of propeller performance, the altitudinal relationship can be quite complicated. Some of the simplifying assumptions include the application of Bernoullis equation for incompressible fluids, the ideal gas law, an assumption of zero humidity, a lapse rate relationship between temperature and altitude (typically only applicable for up to 15 km), and wind velocity is taken to be in the axial direction only. The assumption of an incompressible gas fails at high altitudes. However, pressure is a far more measurable quantity than wind speed near a propeller for experiments performed outside of a wind tunnel. An additional measurement of thrust based on axial strain can be used to better understand the error caused by the assumption of an incompressible fluid. Measurements of the humidity, temperature, and wind velocity/direction can help to determine the validity of some of the other simplifying assumptions. Given the unknown interplay between the different variables in Equation 11 and their relationship with altitude, the efficiency of a particular type of propeller is better determined relative to another type of propeller. In this sense, one can understand which propeller characteristics offer the greatest efficiency benefits as a function of altitude by comparing performance of a propeller with a certain characteristic, to the performance of a propeller with out that characteristic. For instance, one could compare the performance of a highly symmetric airfoil to that of an airfoil with a particular amount of camber in order to understand the effects of camber on airfoil performance as a function of altitude. In order to establish a control for the various environmental conditions represented in Equation 11, it is important to test the two types of airfoils together.

4. PAYLOAD CONCEPT

The High Altitude Turbine Survey (HATS) was proposed as an altitudinal wind velocity experiment aimed at understanding thrust and other performance characteristics along a vertical profile (40 km). On a higher level, the objective of HATS was to perform a feasibility study of how altitudinal turbine airfoil designs can be tested at extended altitudes, where wind strength varies as a function of height. Future work would ideally involve turbine airfoil performance analysis on a larger scale, with a precisely calibrated and customized sensory package.

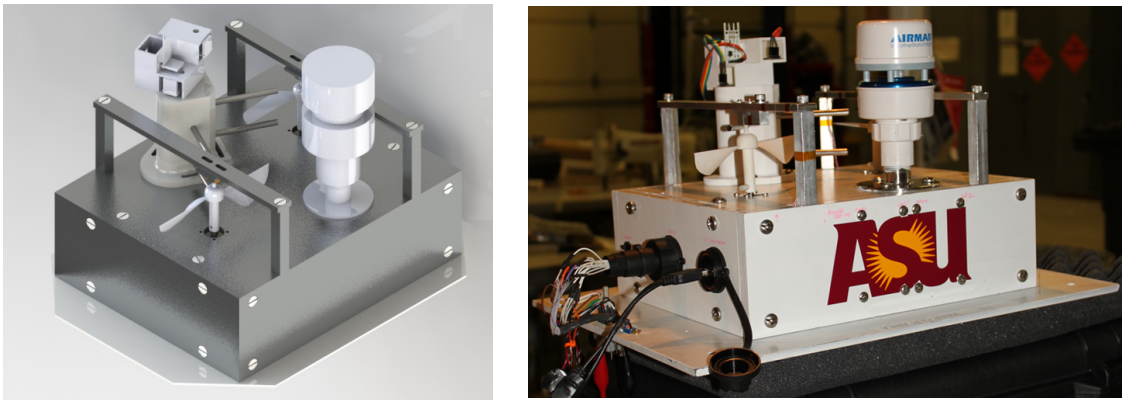

(a) Solid Model **(b)** As Built

Figure 4. Payload Design

As shown in Figure 4*a* above, the payload concept was designed in Solidworks, where individual parameters could be optimized for space and operational efficiency. Figure 4*b* shows the realization of this design as it was being integrated and tested prior to flight. Sensors including optical encoders, strain gauges, thermocouples, pressure gauges, and a digital weather station, all of which are commonly available off the shelf, provided environmental data throughout ascent and descent. The data collected is used to create a velocity and thrust generation profile corresponding to altitude, pressure, and wind speed. Survey findings and, more importantly, engineering lessons, have a wide range of application towards further study, including wind power generation from airborne turbines, propeller-driven airships, and micro-propeller performance characteristics at extended altitudes. The HATS payload was flown on the 2012 NASA High Altitude Student Platform (HASP) in September of 2012. HASP floats to an altitude of 38 km using a specialized high altitude balloon (Weizen W11.82-1E-37).

5. PRINCIPLE OF OPERATION

The system was initiated at launch and data was logged for the entire duration of the ascent, cruise, and descent phases. During the ascent, on-board propellers operated at a single speed, while airfoil performance characteristics, and ambient environmental conditions were measured corresponding to altitude. Once HASP reached the maximum altitude of 38 km, the propellers were operated for an additional 30 minutes until the deactivation, which was necessary to prevent overheating conditions while under vacuum. During the cruise stage, the lack atmosphere and relative wind induces a static condition on the propeller which is not of extended interest, and thus, requires only a limited period of measurement. Environmental data was more relevant in the cruise stage and was collected throughout the flight.

Prior to descent, the propeller motors were powered on in order to provide a secondary comparative thrust/altitude measurement. Once the balloon was released near the end of the flight, HATS descended under parachute in time frame nearly four times shorter than the ascent (thirty minutes versus two hours respectively). This rapid descent caused relative wind motion and subsequent dynamic thrust conditions to be more prevalent on descent. In either circumstance, the movement of HASP with respect to prevailing winds provides a small relative wind velocity across the payload and propeller system. This relative wind allows for dynamic thrust measurements to be recorded at various altitudes.

Throughout the flight, critical data was simultaneously saved to a series of on-board SD cards as well as transmitted to a ground station via the HASP down range wireless communication system. The transmitted data allowed the ground control team to monitor internal temperature and motor status in order to prevent payload malfunction/failure.

6. DESIGN CONSIDERATIONS

The HATS system was designed in accordance with all mass, size, and power requirements according to HASP/NASA protocol. These constraints included a measured system mass of 10 kg (20kg max), a footprint and height of of 38x30 and 26 cm (30 cm max) respectively, and a total power usage of 12-20W (Max 75W) at 30 VDC.

Due to the high altitudes at which the payload operates, design constraints became a factor. In general, the payload was designed to withstand temperatures between -50 and 50 °C, and pressure ranges of 100 kPa at the surface to 0.5 kPa at peak altitude. Extremely low pressures at altitude make convective cooling impossible. Motor choice factors into this, as the heat produced from each core-less brushed motor (1G32E-05K Planetary DC Geared Motor w/ Optical Encoder), which has an average efficiency of approximately 70 percent and average power of 10 W, results in an average heating of 3 W per motor (6 W total). As such, the motors were powered off for the extended low pressure cruise phase. Other heat producing components, such as power systems and on-board processors, were thermally heat-sunk to thick (12.7 mm) aluminum housing walls using copper strips and and a thermal non-conductive epoxy (KONA 870FTLV-DP RESIN). All exterior aluminum was coated in reflective white paint to abate the effects of solar heating. At extreme altitudes, the aluminum box made some heat dissipation possible. In heated conditions, the box prevented extreme temperatures from influencing thermally sunk internal electronics, while in cooled conditions, the latent heat prevented electronics from reaching minimum operating temperatures. System temperature was monitored at key positions on the interior and exterior of the HATS payload via two digital (MAXIM DS18B20) and two analog (AD22100) temperature sensors. Throughout the flight, critical temperature data was available at the ground station. If mission critical functions reached prohibitive temperatures, the system could be powered off remotely in order to prevent failure/damage.

As previously mentioned, the majority of current high altitude wind turbines are not motorized. However these systems are tethered, which is not allowable under HASP requirements or FAA constraints (tethered flight is limited to 500 meters). Although motorized propellers negate some of the effects that an ideal turbine test would exhibit, a motorized system still offers insight into the operation of turbine systems at extended altitudes by allowing for continuous thrust measurements throughout the flight. In order to accommodate the motors on the HATS system, the propellers were top-mounted (negating lateral effects) to allow for maximized propeller diameter and protection of the electronic hardware below.

7. AIRFOIL DESIGN

The objective of the HATS experiment required that two distinctly designed propellers with different performance characteristics be used in order to assess thrust efficiency at varying altitude. Due to payload size limitations, propeller radius was limited, and so down-scaling was necessary. Size limitations allowed for a maximized radius of 7.62cm (15.24cm diameter) for each propeller. While it is understood that efficiency and performance characteristics of micro-propellers are not quantitatively scalable to larger versions, this experiment is more focused on developing a high altitude turbine airfoil testing platform for future studies on such scales.

The National Advisory Committee for Aeronautics (NACA) offers an online airfoil database were standardized and tested propeller designs can be found. The NACA 0012 airfoil (00 = symmetry, 12 = thickness) was suited for low altitude

aviation applications, and was selected as our standard model. The NACA 0012 (shown in Figure 5*a*) has a diminished performance at high altitudes. Accordingly, this airfoil, whose performance characteristics are well understood at lower altitudes, should fail in comparison to a high altitude optimized airfoil design. The search for high altitude airfoil designs within the NACA design database produced no potential candidates, as the majority of designs had been optimized for lower altitudes common to standard aircraft flight.

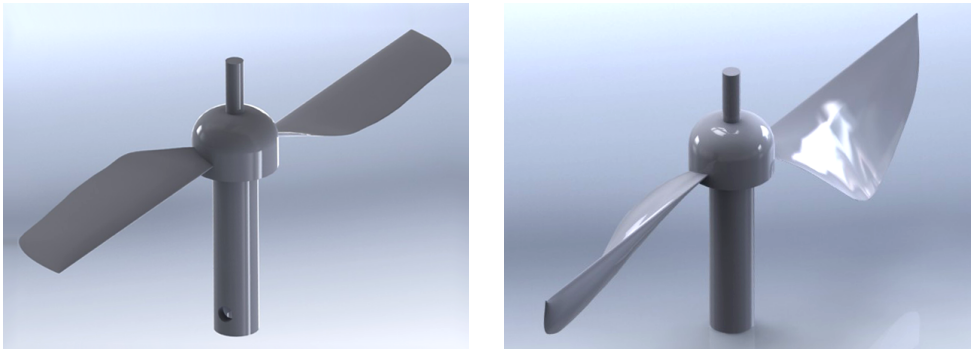

(a) NACA-12 **(b)** APEX-16

Figure 5. Airfoil Designs

In order to find a suitable high altitude airfoil, we turned to a conceptual design study performed by NASA Dryden Flight Research Center [8]. The NASA APEX project was commissioned to engineer an ultralight fixed-wing aircraft that could be balloon launched and operated at altitudes above 30 km for high altitude sustained flight [8]. The APEX-16 airfoil (shown in Figure 5*b*) was designed to be used in the APEX project, and was optimized for use at altitudes where low Reynolds numbers (inertial to viscous force ratio) and high subsonic Mach numbers (velocity to speed of sound ratio) prevail. Unfortunately, the NASA APEX project was canceled prior to test flights, so the APEX-16 was never actually flown at high altitudes. In spite of project cancellation, APEX-16 performance modeling illustrates operating capacity at high altitudes [8]. Using numerical airfoil modeling data from the APEX project, a scaled version of the APEX-16 was created.

The propellers were generated using airfoil coordinates, radial twist functions, and radial chord functions. The APEX-16 coordinates and radius functions were obtained from reference [8]. The NACA 0012 data was obtained from an online NACA database and a standard $1/r^2$ twist function was assumed. A MATLAB script was then used to translate these functions to 3D coordinates, which were then imported into Solidworks to generate 3D propeller models. Finally these design were sent to Shapeways, where 3D Printed plastic models were created. 3D printing made it possible to fabricate small, customized propellers, which conformed to the much larger designs of the NACA 0012 and APEX-16 airfoils.

8. SENSORS AND DATA COLLECTION

Pressure Sensors

Propeller thrust can be determined with pressure sensors. In this case, two absolute pressure sensors (Honeywell ASDX015A24R), mounted before and after each propeller (Figure 6*b*), can be used to measure the pressure drop across the propeller, which can then be converted into an estimation of propeller thrust as described in Section 3.

Average pressure is more important than instantaneous pressure in calculating thrust, and given the 125 Hz maximum operational frequency of the sensor, the propeller speed could not exceed 31 RPS (1,860 RPM). This is the case because each time the propeller blade passes over the pressure sensor, the sensor will record a spike or drop in pressure depending on sensor placement. When the sensor records a data point that is not over the propeller blade it will be a different value. Neither of these values is equivalent to the pressure before or after the propeller. Instead, the desired value is the average pressure over the disk swept by the propeller before and after. Accurate measurement of continuous propeller pressure requires at least 4 samples per rotation given our dual blade configuration. These pressure readings can then be averaged in order to obtain the desired results. In response to this, our maximum propeller speed was set to 20 RPS (1,200 RPM).

In addition to four performance pressure sensors, an additional sensor was used to measure the ambient pressure conditions throughout the flight. The ambient pressure sensor was used to calculate the altitude of the payload by comparison to an atmospheric model. This data was then compared to the GPS data collected from the HASP system. The ambient pressure sensor data is also utilized to determine the approximate density of the atmosphere for a given set of data measurements.

(a) Propeller Assembly

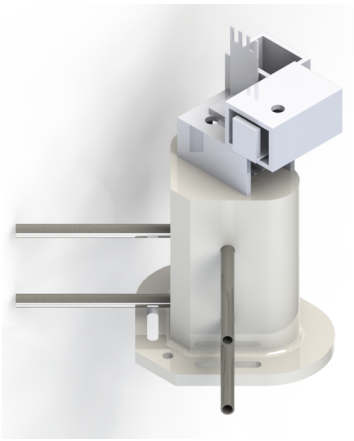

(b) Prop Pressure w/ Axial Anemometer

(c) Airmar PB200 Weather Station

Figure 6. Sensor Package

Strain Gauges

Due to compressibility and accuracy concerns with pressure gauges, strain gauges were also mounted along the propeller shaft in order to provide an alternative thrust measurement. Equation 12 provides the relationship between thrust and strain.

$$T = \epsilon \cdot Young's Modulus \cdot Area \tag{12}$$

Due to the small size of the propellers and their shafts, the strain gauges could not be mounted directly on the shaft. As shown in Figure 6*a*, two bi-axial strain gauges (Omega SGK-B5A-K350W-PC23-E) are affixed to either side of the of the mount. As such, the area in Equation 12 is not the area of the shaft but rather the cross-sectional area of the strain gauge mount (approximately $1.65{*}10^{-2}$ m^2). Due to the small magnitude of the anticipated thrust force, the size of the strain gauge mount was minimized to the minimum dimensions allowable to provide sufficient contact and support for the strain gauges. The material used for the strain gauge mount was aluminum 6061, which has a Youngs Modulus of approximately 69 GPa. The strain gauges were mounted to the propeller assembly in a full Wheatstone bridge arrangement. This was done to compensate for any temperature or lateral forces. In this arrangement, assuming a balanced bridge, the strain in the assembly can be calculated as shown in Equation 13.

$$\frac{V_0}{V_{ex}} = -GF \cdot \epsilon \tag{13}$$

V_0 is the output voltage of the strain gauge, V_{ex} is the excitation voltage or voltage applied to the gauge (approximately 5V), and GF is the gauge factor (approximately 2 for metal strain gauges). From Equation 12, the thrust of the propellers can be determined as shown in Equation 14.

$$T = \frac{-2}{5} \cdot V_0 \cdot 69 \cdot 10^9 \cdot 1.65 \cdot 10^{-2} \approx -4.56 \cdot 10^8 \cdot V_0 \tag{14}$$

Weather Station

The AIRMAR PB200 weather station (shown in Figure 6*c*) provides both absolute and relative wind velocities, enabling a complete picture of wind speed throughout its operation. Wind velocity data is most sensitive laterally in the x and y dimension. The PB200 also serves as a redundancy check for other systems (temperature, pressure, etc.), as it features a host of sensors common to marine use.

Traditionally, high altitude wind speeds are measured using radiosondes mounted on weather balloons. These devices send a signal to a ground station and measure the frequency shift to estimate the change in velocity. However, this provides only the absolute velocity of the balloon. The Airmar PB200 is used to account for relative wind motion near the propellers. Propeller performance is greatly impacted by wind conditions, as wind velocities at high altitudes are more than adequate for high altitude power generation. Unfortunately, the balloon-borne HATS payload experiences small relative lateral wind velocities due to trajectory acclimation with prevailing winds. Nevertheless, even small wind velocities require characterization in order to account for potential impact on the payload.

Axial Anemometer

The Airmar PB200 is most sensitive to lateral wind movement, so an alternative thermisistor type anemometer was utilized to sample wind velocities in a vertical manner. Four Modern Device MD0550 sensors were used in a mutli-axis configuration. This configuration not only allowed for characterization of the vertical wind component (z-direction), but served as a backup for the Airmar PB200 in in cases where wind movement was minimal. The orientation of these sensors was critical to understanding wind velocities during flight. Three anemometers were used to record wind magnitudes from three isolated axes (x,y,z) while one anemometer was open to all directions, as shown in Figure 6*b*.

Data Collection / Payload Control

The HATS payload uses an on-board central micro-controller (Arduino Mega), which facilitates data collection, instrument control, and communication throughout the flight. The micro-controller is also connected to the HASP ground station transmitter via a supplied serial port with a 4800 Baud connection. Data from the weather station and Arduino are written to separate SD card loggers which write data at 4800 and 19200 baud respectively. HATS sensory data is pulled and recorded at 20 Hz, a rate set by the pressure gauge's maximum sampling rate.

9. FLIGHT DATA ANALYSIS

Weather Station

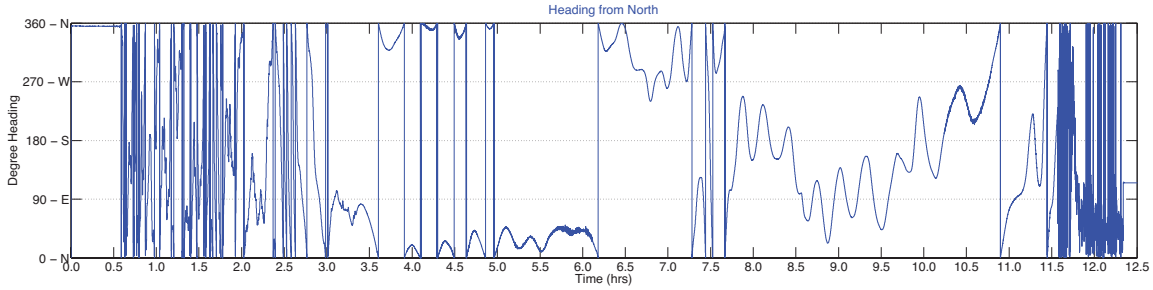

Figure 7. Payload Heading North

Directional Heading - The Airmar BP200 magnetic heading reading indicates payload orientation with respect to North. Figure 7 illustrates magnetic heading data over 12.5 hours of payload operation. It should be noted that the 12.5 hour data collection includes time spent on the ground during take-off and landing. Total flight time was 11.5 hours, encompassing both take-off (0.5 - 2.5 hr mark) and landing (11.75 - 12.25 hr mark). These phases are indicative of rapid changes in magnetic heading. The cruise phase (2.5 - 11.75 hr mark) shows continued heading variance at reduced rates. Any straight vertical lines in the data correlate to the transition between N-W and N-E headings. At no point in the flight was the payload yaw motion unidirectional. Even during the cruise phase, the HASP payload alternates spin direction on 10-20 minute intervals.

Yaw Rate - Figure 8 shows the yaw rate over 12.5 hours of operation. The rotational rate is described in rotations per minute (RPM) and is referenced by the internal magnetic compass on the Airmar PB200. The ascent and descent phases exhibit greater rotational rates than the cruise phase as expected. The rate modulation is greatest during descent (11.75 - 12.25 hr mark), due to turbulence experienced from free fall through landing under parachute. At free fall, a maximum yaw rate of 9 - 10 RPM is achieved. Once the payload stabilizes under parachute, the rate falls to 1 - 3 RPM until touchdown. The ascent phase (0.5 - 2.5 hr mark) is marked by a steady 0.5 - 1.5 RPM rotation with peaks at 2 RPM. During the cruise phase (2.5 - 11.75 hr mark) the yaw rate is at a minimum (zero with minor fluctuations). These rates may appear to contradict directional heading data, but it is important to note that the yaw motion was not unidirectional or rapid during this period. Slow rotational rates do not indicate a lack of directional variation, but rather, a lack of resolution on the scale of revolutions every minute.

Payload Pitch - Figure 9 illustrates the variance of the payload with respect to the horizon in degrees. Near the 0.5 hour mark the payload was launched and a subsequent spike in pitch is recorded. From this point the pitch is generally steady,

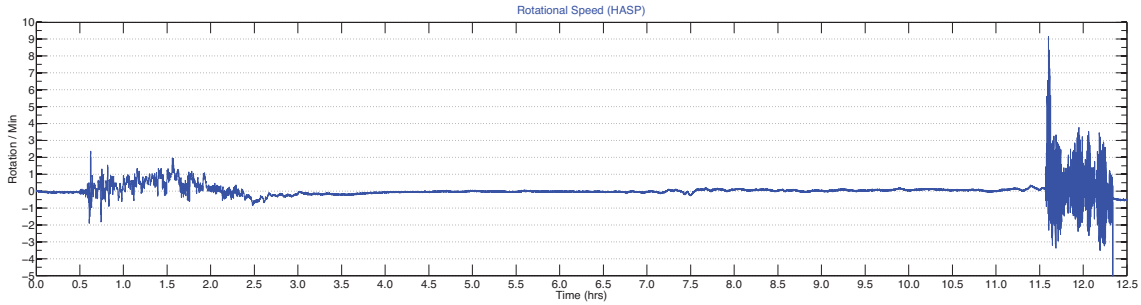

Figure 8. Payload Rotation (degrees per minute)

with no more than a degree in inclination until the 4 hour mark. Collective pitch readings from hours 4 though 11.5 do not correspond to to actual movement and are likely the result of instrument malfunction. The malfunction period is marked by extreme temperature variations and diminished pressure, which may have caused instrument failure. The descent phase, which exhibits lower temperatures and increased pressures, appears to mark the recovery of the accelerometer pitch accuracy.

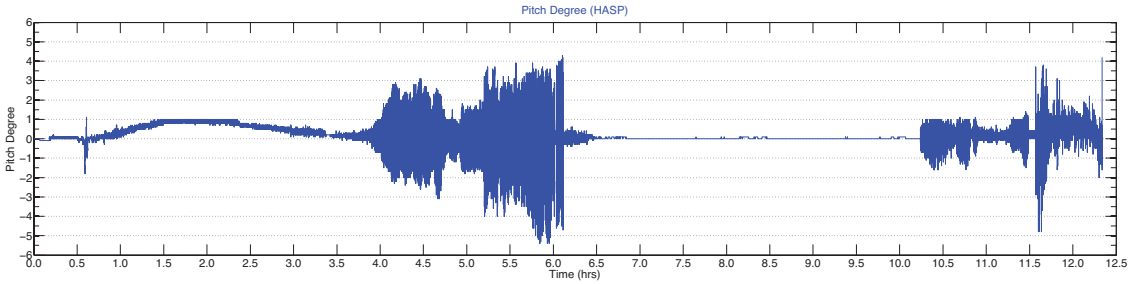

Figure 9. Payload Pitch

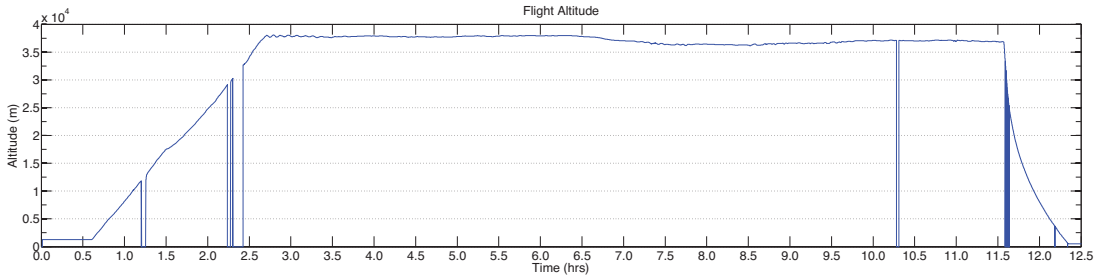

Figure 10. Payload Flight Altitude

GPS Altitude - GPS was used to determine flight altitude and position over ground. Figure 10 displays the altitude over time for the entire mission operation. The ascent and descent are shown to occur over both 2 hour and 45 minute intervals respectively, with a total cruise time of over 9 hours. The max altitude reached was shown to be 38 km occurring during the early stages of the cruise phase. Most commercial GPS units have an imposed altitude and velocity restriction of 18.3 km and 1,852 km/h respectively. While the limit of altitude is exceeded, the accuracy of the GPS altitude reading is consistent with both the expected max float altitude and measurements taken by HASP.

GPS Heading - While the GPS Altitude reading appears to be accurate, the position over ground shown in Figure 11*a* shows a lack of accuracy versus the HASP provided Google GPS track (Figure 11*b*). The GPS failed to capture

longitudinal and latitudinal data accurately over the course of the flight. The launch coordinates for the Ft. Sumner launch site in New Mexico are known to be 34.49°N,-104.22°W. The Airmar PB200 GPS data show an initial lunch location of 33.75°N,-108.55°W, which is more than 450 km to the west of Ft. Sumner, NM. The landing occurred at the known location of 33.74°N,-112.78°W (Toyota Proving Grounds, AZ). Again the Airmar PB200 GPS data showed inaccuracies, but this time the true location was off by less than 30km. While GPS position data is insignificant to the mission objective, altitude data is relevant. As such, altitude was inferred from pressure data with reference to the 1976 Standard Atmospheric Model [10]

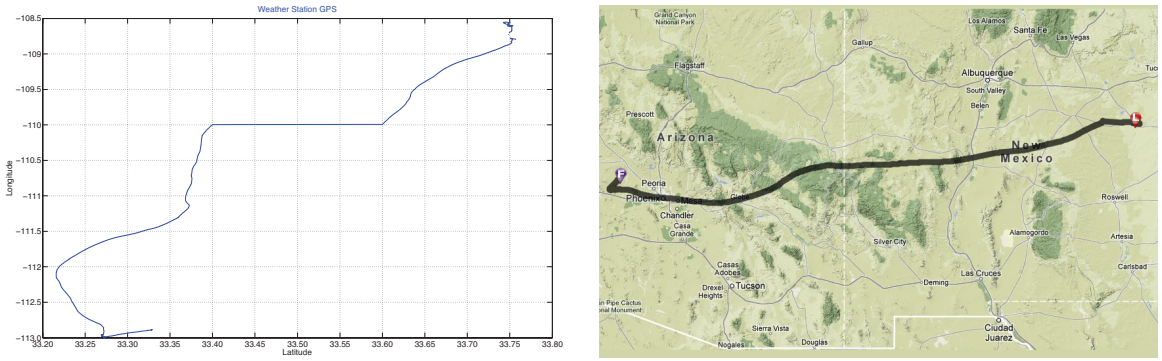

(a) Weather Station GPS

(b) HASP Google GPS Track rep.[14]

Figure 11. GPS Track

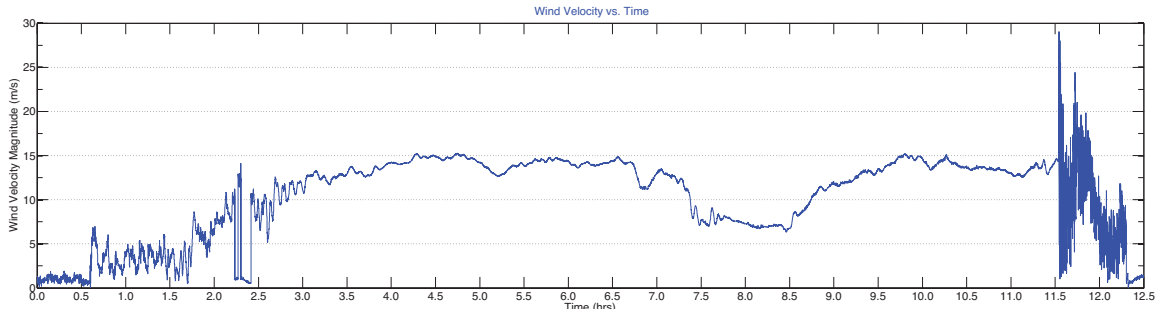

Figure 12. Wind Speed (m/s)

Wind Speed - Figure 12 illustrates the absolute wind speed (m/s) as measured by the ultrasonic anemometer. Due to some issues with the interfacing between the HATS system and the Airmar PB200 sensor, a sub-optimal method for velocity calculation was implemented. In this method, the resolution is such that null values are recorded in between true data points, resulting in an erroneous alteration of the wind speed measurements. Integrating wind speed over time should yield an estimation of distance. After correcting for some of the data collection anomalies, the wind speed measurements indicate that the system should have traveled approximately 950 km as compared to the 892 km total distance recorded by the HASP system. This discrepancy would indicate that the airmar sensor was recording higher wind velocities than were actually occurring. It should be noted that the wind speed data has not been corrected for the influence from HASP payload rotation. However, it is expected that this contribution should be small. Alternatively, by comparing the wind speed data recorded by the Airmar sensor with the wind profile shown in figure 2, it can be seen that the Airmar sensor was recording velocities that were much higher than anticipated particularly at altitude during the cruise phase. Previously, the Airmar had only been operated to a maximum altitude of 8 km. Given that the sensor uses an ultrasonic measurement to analyze wind velocity, the higher than expected wind velocities at high altitudes may be the result of the greatly reduced density at these altitudes. As density decreases, the speed of the ultrasonic pulse would increase leading to an overestimate of the wind velocity. From, this data it can be concluded that the Airmar ultrasonic anemometer is insufficient for velocity measurements at such extreme altitudes. Alternatively, the wind speed data collected during ascent and descent may be more reliable. Yet from figure 12, no obvious indications of the high velocity jet stream data can be seen during ascent while there are discernible peaks during the descent phase. This lack of data may be tied to the rate at which the sensor

setting was collecting data compared to the rate at which the system was changing altitude. In order to better characterize the performance of the Airmar wind sensor, a more capable sensor should be used on future flights for comparison.

Relative Wind Angle - The inclination of prevailing winds relative to the horizontal payload is shown in Figure 13. The ascent and descent phases show a large amount of variability, which was expected due to the prevalence of increased wind turbulence in both lateral and vertical directions. Characteristic jet stream wind turbulence is possibly shown from the 0.5 - 1.25 hr mark, where the wind angle is most variable. The negative wind attack angle was consistent throughout the cruise phase (1.25 - 11.5 hr mark), which could be indicative of either constant upward wind motion or the instruments failure to characterize wind with limited pressure and extreme temperature variation. The descent phase (11.5 -12.5 hr mark) shows high variability, but it is not possible to discern jet stream activity from the effects of free-fall and landing under parachute.

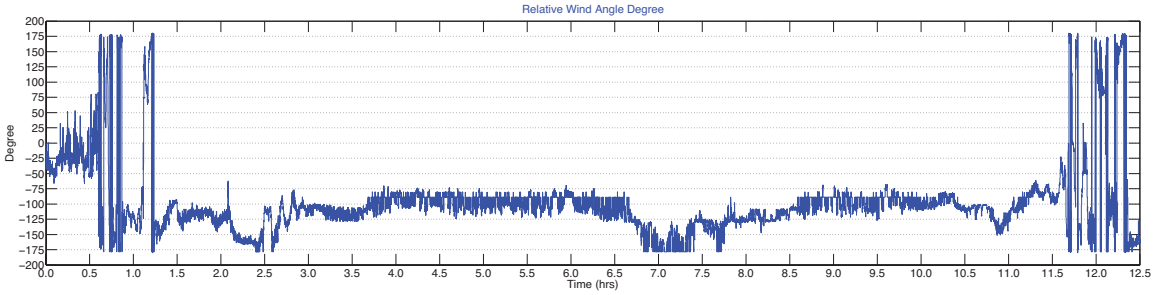

Figure 13. Relative Wind Angle

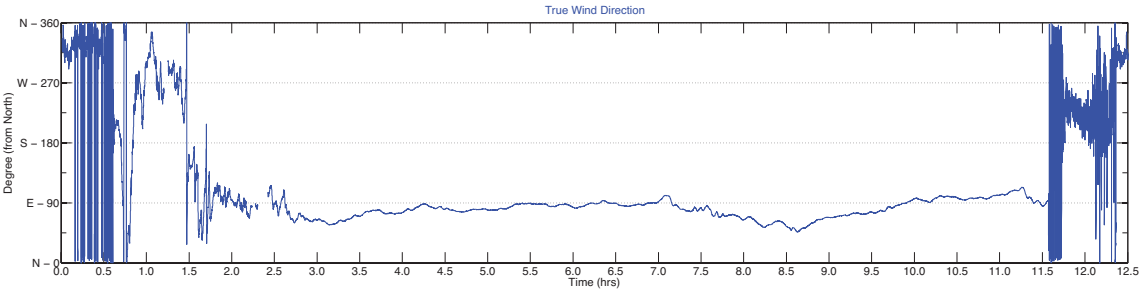

Figure 14. True Wind Direction

True Wind Direction - The ultrasonic anemometer characterized true wind direction as shown in Figure 14. This measurement is discerned by associating anemometer input with magnetic compass heading, which is a calibrated feature of the Airmar PB200. The most significant attribute of this data was the prevalence of an easterly wind with some influence from the north. This is to be expected and is indicative of the westerly flight path of HASP shown in Figure 11*b*.

Ambient Sensor Data

Atmospheric Pressure - Ambient pressure data provides a direct altitude correlation to the 1976 Standard Atmospheric Model [10] (reproduced in Figure 15*a*) during ascent and descent. Figure 15*b* shows the pressure data in kPa over the course of the flight. The data follows expected pressure regimes until the cruise phase. The pressure data indicates a minimum of 10 kPa during the cruise phase, which is 9.5 kPa greater than expected pressure (0.5 kPa according to HASP environmental readings). Failure to measure the precise minimum pressure at altitude could be the result of the sensor operating outside of temperature constraints and or the lack of accuracy at extraordinarily low pressures. 10.

Temperature - Figure 16 shows temperature measurements at several key payload locations. Analog sensors (AD22100) were used to characterize interior and exterior ambient temperatures, while digital sensors (DS18B20) recorded operating temperatures for a single motor and 12 V power supply. Ambient temperature data follows expected trends with the insulated interior being relatively stable in comparison to the fluctuations in exterior data. It should be noted that the

external temperature data exhibits an undesired resonance, likely due to electrical noise. The system power supply and motor temperature generally follow overall fluctuations. The motor, when in operation, generally exhibits a relative maximum in temperature. Given the power inefficiency of brushed motors, this result was expected.

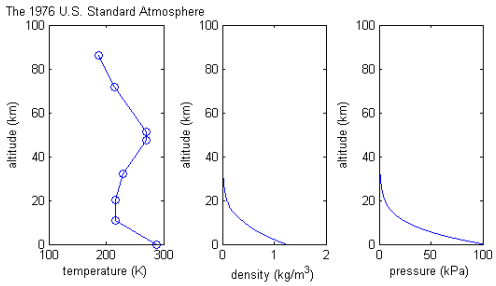

(a) 1976 Standard Atmospheric Model rep.[16]

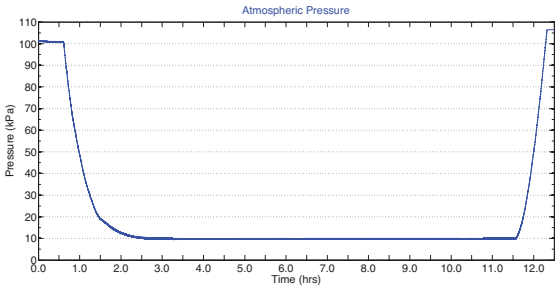

(b) Atmospheric Pressure (kPa)

Figure 15. Atmospheric Data

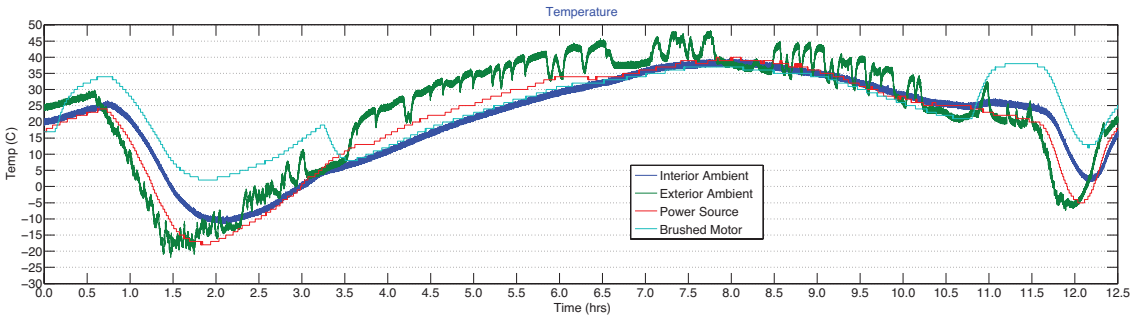

Figure 16. Flight Temperatures

Axial Anemometer - The axial anemometer was an experimental wind measurement device composed of 4 off-the-shelf hot wire anemometer chips. The successful operation of this sensory device was not critical to data analysis, but was rather a technology demonstration of an unproven technique in axial wind measurement. Figure 17 shows the recorded wind data with respect to time for the four individual sensors. While the data output for each sensor follows a general trend, the expected directionality of the wind is not discernible. The isolated X,Y,and Z data sets are not indicative of a changing wind direction, but rather, of an inverse temperature measurement. Hot-wire anemometers are temperature dependent and their use in an environment with such drastic and extreme variation did not befit their ideal use.

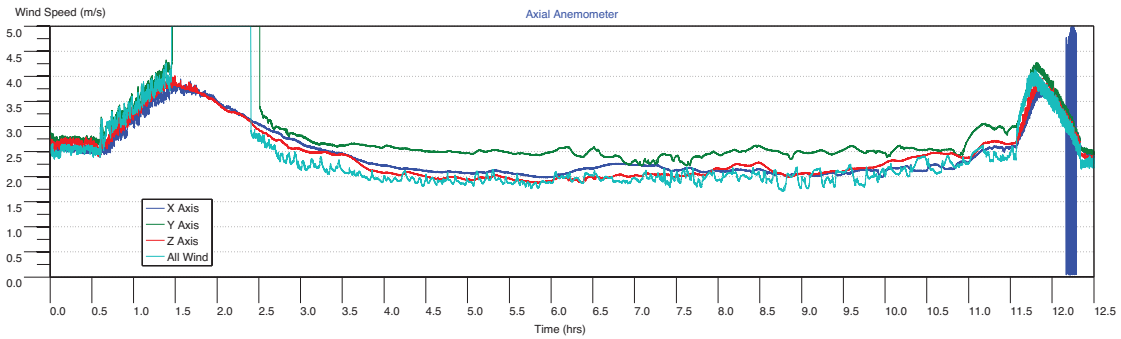

Figure 17. Axial Anemometer

Performance Analysis

The relation of propeller efficiency to atmospheric variability is dependent upon measured performance data, upward payload velocity, and density assumptions from the 1976 Standard Atmospheric Model [10]. Due to problems outlined in Section 10, strain data was not factored into efficiency calculations. Pressure measurements comprise the only available propeller performance data, and were used to calculate only NACA 0012 efficiency. No efficiency comparisons can be made between the NACA 0012 and APEX-16 airfoil designs because the APEX-16 pressure differential ADC (analog to digital converter) appears to have sustained electrical damage at some point prior to or during the flight. While we can not say with absolute certainty that NACA 0012 efficiency data supports the effective use of this type of differential propeller pressure measurements as a means to measure or compare performance at altitude, the findings appear to support general efficiency assumptions. It should be noted that using an idealized mathematical efficiency model (Eqn.11) may oversimplify the problem, and not be representative of true propeller performance.

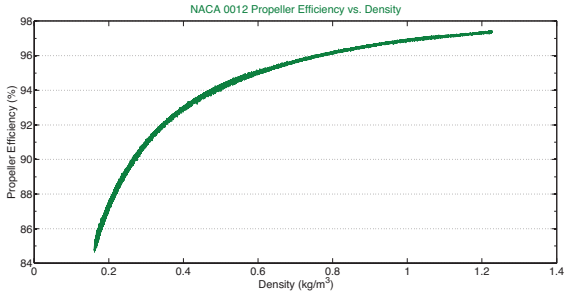

(a) Efficiency vs. Atmospheric Density [10]

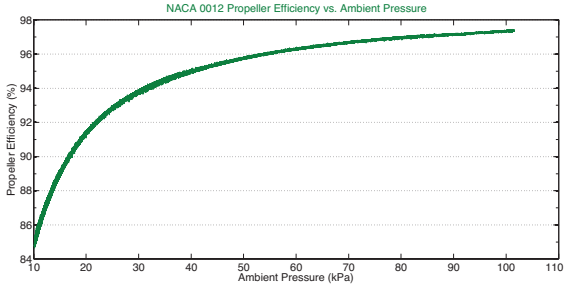

(b) Efficiency vs. Ambient Pressure

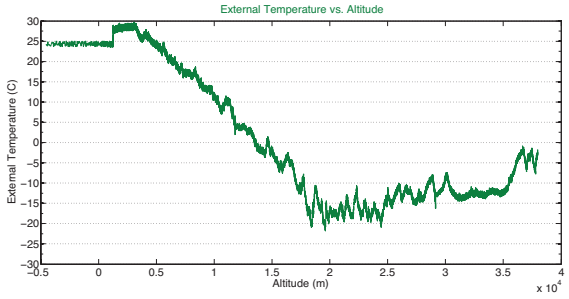

(c) Temperature vs. Altitude

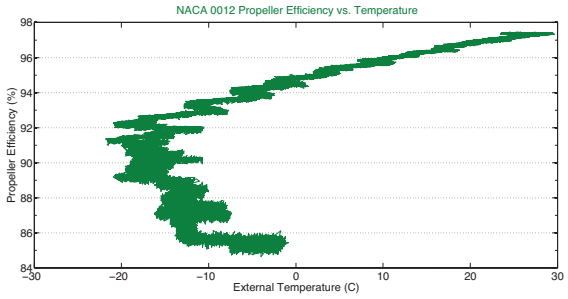

(d) Efficiency vs. External Temperature

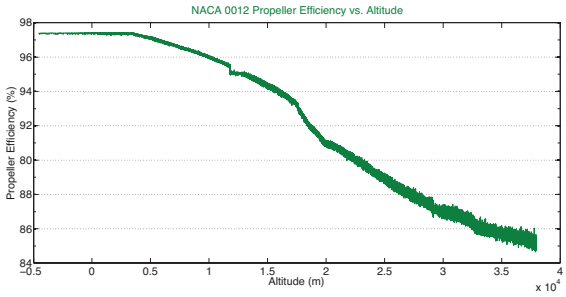

(e) Efficiency vs. Altitude

Figure 18. Efficiency Analysis (NACA 0012 Shown)

Figure 18*a* and Figure 18*b* represent the percentage efficiency of the NACA 012 airfoil with respect to recorded ambient pressure and atmospheric density as predicated by the 1976 Standard Atmospheric Model [10]. Efficiency appears to follow an expected relationship of altitudinal propeller performance.

At lower altitudes, Figure 18*c* illustrates the standard linear lapse rate temperature versus altitude dependence. As the payload approaches approximately 20km, the upper limit of the troposphere, the linear relationship degrades as expected. Interestingly, this shift from a linear temperature relationship at around 20km corresponds to a change in concavity in the efficiency versus altitude plot (Figure 18*e*). Figure 18*d* directly compares the impact of temperature on efficiency. Given the varying relationship, it can be assumed that the efficiency data does not correlate to temperature as would be expected if the pressure sensors were not functioning properly at low temperatures.

10. FAILURE ANALYSIS

The flight data was indicative of several notable instrument failures resulting in erroneous data and even loss of measurements. Propeller performance data was reliant upon a set of pressure and strain gauges which used 16 bit differential dual input analog to digital (ADC) conversion chips (TI ADS115). The ADC allowed for a differential resolution of 65,535 digital values at a preset voltage constraint. For example, the strain gauges were constrained to a range of $\pm$ 6.144 VDC with a resolution of 1 digital value for every $1.875*10^{-4}$ volt. Pressure gauge input ranges were constrained to $\pm$ 0.256 VDC with a resolution of 1 digital value for every $7.813*10^{-6}$ volt. Grounding issues, resulting from unmitigated electrical charge build up in the aluminum housing, may have caused ADC failure for the APEX-16 set of pressure and strain gauges. We can assume this error from differential data readings, which were pinned at max value for the duration of the flight. Another possible failure scenario would be ADC chip damage from extreme temperature and pressure cycling in thermal vacuum tests prior to flight. In addition to this, the NACA 0012 strain gauge system suffered physical damage from exposure to repeated heating and cooling cycles. It is not known exactly when the break occurred, but the result was obvious in errant data variation.

The Airmar PB200 weather station produced useful data related to platform orientation and wind characterization. However, particular sensor readings within the recorded NMEA 0183 string (marine data protocol) produced null values. Null data was recorded for variables such as humidity, temperature, and relative wind speed. The collection failure resulted from the use of an improper data/voltage conversion circuit, namely the RS-232. For the Airmar PB200 to properly export all calibrated data, a RS-422 conversion should have been used, as it allows for a greater communication baud rate (38,400 baud). Using an RS-232 connection limits the baud rate to 4800 baud, meaning any data sets requiring higher transfer rates were lost. This problem was known prior to flight and was not addressed because using an RS-422 connection would also require using a different NMEA protocol (NMEA 2000). To read and write NMEA 2000 data would have required the use of a single-board computer to record data. Using an on-board computer was considered to critical risk due to processor overheating concerns in pressure reduced environments. With that said, the use of the Airmar PB200 was entirely experimental. The device had not been factory tested to the temperature, pressure, and altitude extremes experienced in the HASP flight, and clearly demonstrated measurement errors as a result. Although an ultrasonic multi-sensor instrument is beneficial to high altitude flight characterization, a more robust sensor would likely yield more accurate results.

11. FUTURE WORK

Future research would entail the systematic development of a full-scale high altitudinal airfoil turbine test platform and wind turbine efficiency database. The performance database would be made available to researchers and industry professionals involved with airborne wind energy research. Creating a database of high altitude airfoil designs and performance characteristics would enable researchers to more effectively identify aerodynamic surfaces and designs better suited to desired operating conditions. This program will involve a combination of computational modeling, wind tunnel analysis, and field testing in order to provide the basic tools necessary for future development.

REFERENCES

1. Bolonkin, A. Using of high altitude wind energy, Smart Grid and Renewable Energy, 2(2), 75-85, May 2011.
2. Bronstein, M. G., Harnessing rivers of wind: A technology and policy assessment of high altitude wind power in the U.S., Technological Forecasting and Social Change, 78 (4), 736- 746, 2011.
3. Davidson, K., Scientists look high in the sky for power, The San Francisco Chronicle, A-1, 7 May 2007.
4. Grasso, F., Usage of Numerical Optimization in Wind Turbine Airfoil Design, Journal of Aircraft, 48 (1), 248-255, 2011.
5. A.E. Hedin, E.L. Fleming, A.H. Manson, F.J. Schmidlin, S.K. Avery, R.R. Clark, S.J. Franke, G.J. Fraser, T. Tsuda, F. Vial, R.A. Vincent, Empirical wind model for the upper, middle and lower atmosphere, Journal of Atmospheric and Terrestrial Physics, 58(13), 1421-1447, September 1996.
6. Herbert, G.M.J., Iniyan, S., Sreevalsan, E., Rajapandian, S., A review of wind energy technologies, Renewable and Sustainable Energy Reviews, 11 (6), 1117-1145, 2007.
7. Houghton, E. L., and P. W. Carpenter. "Ch.9." Aerodynamics for Engineering Students. Oxford: Butterworth-Heinemann, 2003. 528.
8. Murray, J., Moes, T., Norlin, K., Bauer, J., Geenen, R., Moulton, B., Hoang, S., "Piloted Simulation Study of a Balloon-Assisted Deployment of an Aircraft at High Altitude", NASA TM 104245, January 1992.
9. Roberts, B.W., Shepard, D.H., Caldeira, K., Cannon, M.E., Eccles, D.G., Grenier, A.J., Freidin, J.F., "Harnessing High-Altitude Wind Power," Transactions on Energy Conversion, IEEE , 22 (1), 136-144, March 2007.
10. U.S. Standard Atmosphere, 1976, U.S. Government Printing Office, Washington, D.C., 1976.
11. www.airmartechnology.com
12. www.altaerosenergies.com
13. www.jpaerospace.com/atohandout.pdf
14. www.laspace.lsu.edu/hasp/
15. www.moderndevice.com
16. www.pdas.com/programs/atmos.f90
17. www.skywindpower.com
18. www.windenergy.com/products/skystream